

Low-dimensional modelling of a confined three-dimensional wake flow

By M. BUFFONI^{1,3}, S. CAMARRI², A. IOLLO³
AND M. V. SALVETTI²

¹Dipartimento di Ingegneria Aeronautica e Spaziale, Politecnico di Torino, 10129 Torino, Italy

²Dipartimento di Ingegneria Aerospaziale, Università di Pisa, 56122 Pisa, Italy

³Mathématiques Appliquées de Bordeaux UMR 5466 CNRS, Université Bordeaux 1, et INRIA Projet MC2, 33405 Talence, France

(Received 3 April 2006 and in revised form 9 September 2006)

The laminar flow past a square cylinder symmetrically placed between two parallel walls is considered. A classical vortex wake is shed from the cylinder, but three-dimensional instabilities are present and they develop in complicated flow patterns. The possibility of extracting an accurate low-order model of this flow is explored.

1. Introduction

Since the introduction in fluid mechanics of model reduction ideas (Lumley 1967), one of the main concerns is to use small-dimensional surrogates to replace the Navier–Stokes equations for control purposes. One application often targeted is the control of vortex shedding (Graham, Peraire & Tang 1998); the benefits of such technology range from reduced fatigue on materials and lower noise emissions, to flight of thick-wing airships. Though examples of vortex shedding control built on low-order models and solid optimization grounds have recently appeared (Bergmann, Cordier & Brancher 2005), they are limited to two-dimensional laminar flows. One of the reasons is that low-order models based on straightforward Galerkin projection over empirical eigenmodes and *ad hoc* additional dissipation fail to represent the correct dynamics if it is not a simple oscillation. Also it is not clear if a low-dimensional representation of more complex flows can be found, and there are examples where such a representation does not exist (Telib, Manhart & Iollo 2004).

In this contribution two possibilities are investigated: (i) providing a small-dimensional representation of a fairly complicated flow and (ii) deriving an accurate dynamical model from such a representation. Ma & Karniadakis (2002) and Galletti *et al.* (2004, 2005) addressed similar questions for simpler flows. Here we investigate the capability of the pseudo-spectral calibration approach introduced in Galletti *et al.* (2005) to model a more complex flow (three-dimensional and non-periodic) than those in the previous investigations. We concentrate on the case of a square cylinder placed at the midspan between two parallel flat walls. The Reynolds numbers considered are such that the flow is characterized by a three-dimensional vortex wake that interferes with the upper and lower walls. Such a configuration has been briefly considered in the literature. As a complement to existing experimental, two-dimensional or theoretical studies, we investigated this flow by direct numerical simulation.

The first part of this paper is therefore a description of the numerical set-up and an analysis of the results obtained. Then, low-order models of the impulsive start-up as well as of the developed flow regimes are investigated.

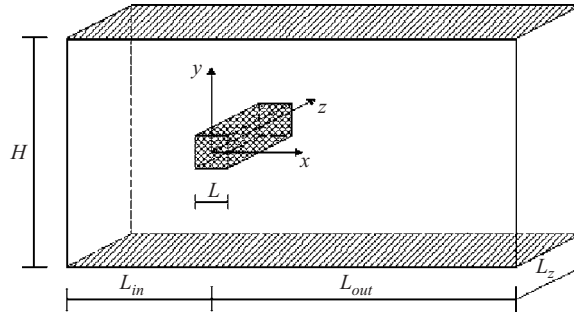


FIGURE 1. Computational domain.

2. Numerical simulation

The configuration used is sketched in figure 1. The ratio between the cylinder side length L and the distance between the walls H is $L/H = 1/8$. The incoming flow is a laminar Poiseuille flow in the x -direction and the Reynolds numbers, based on the maximum velocity of the incoming flow and on L , range between 100 and 300.

For brevity, we only summarize here the main features of the numerical solver employed in the simulations; more details can be found in Camarri *et al.* (2004) and Farhat, Koobus & Tran (1999). The Navier–Stokes equations for compressible flows are discretized in space using a mixed finite-volume/finite-element method applied to unstructured tetrahedrizations. Linear Galerkin finite elements are used to discretize the diffusive terms, while the discretization of the convective terms is carried out through a finite-volume approach on cells built around each vertex of the grid. The finite-volume fluxes through the common boundaries shared by neighbouring cells are approximated by using the upwind Roe scheme (Roe 1981), together with the MUSCL linear reconstruction method (‘Monotone Upwind Schemes for Conservation Laws’, van Leer 1977), in order to obtain second-order accuracy in space. Furthermore, a Turkel-type preconditioning term is introduced to avoid the accuracy problems typical of compressible flow solvers at low Mach numbers (Guillard & Viozat 1999). The time-marching algorithm is implicit and second-order accurate.

The method of characteristics is used to impose non-reflective inflow and outflow boundary conditions. At the inflow the Poiseuille flow is assumed to be undisturbed. Periodic boundary conditions are imposed in the spanwise direction and no-slip conditions are forced on the cylinder and on the parallel walls.

Two different computational domains were used, for carrying out two-dimensional and three-dimensional simulations, which differ only in the spanwise extent of the domain. In both cases, with reference to figure 1, $L_{in}/L = 12$ and $L_{out}/L = 20$. For two-dimensional simulations, the spanwise length adopted is $L_z/L = 0.6$, and it was systematically checked that the simulated spanwise velocity was negligible. For the three-dimensional simulations, the spanwise length of the domain is $L_z/L = 6$. This value was selected following the experimental results for unconfined square-cylinder flow (Luo, Chew & Ng 2003), which show a maximum spanwise length of the three-dimensional structures equal to $5.2L$, and the indications given in Sohankar, Norberg & Davidson (1999) and Saha, Biswas & Muralidhar (2003) for the numerical study of the three-dimensional wake instabilities of a square cylinder in an open uniform flow.

	Re	St	\bar{C}_D	A_{C_D}	A_{C_L}	Re	St	\bar{C}_D	A_{C_D}	A_{C_L}
GR1	100	0.1368	1.3758	0.0065	0.3715	180	0.1404	1.3659	0.0463	0.9303
GR3	100	0.1362	1.3820	0.0066	0.3638	180	0.1388	1.3803	0.0459	0.9423
Breuer <i>et al.</i>	100	0.1391	1.3500	0.0077	0.3835	180	0.1440	1.3250	0.0490	0.9090
Galletti <i>et al.</i>	100	0.1386	–	–	–	180	0.1370	–	–	–

	Re	St	\bar{C}_D	A_{C_D}	A_{C_L}	Number of nodes	Nodes on cylinder perim.	L_z/L
GR1	300	0.1250	1.6205	0.4889	3.4019	7.5×10^5	250	0.6
GR2	300	0.1234	1.6359	0.5151	3.4635	6.6×10^5	210	0.6
GR3	300	0.1237	1.6509	0.5191	3.4807	6.0×10^5	170	0.6
GR4(3D)	300	0.1345	1.4596	0.0876	1.1889	6.6×10^6	250	6.0
Breuer <i>et al.</i>	300	0.1271	1.8603	0.5081	3.3534	1.904×10^5	100	–
Galletti <i>et al.</i>	300	0.1320	–	–	–	$\approx 2.5 \times 10^5$	128	–

TABLE 1. Main bulk coefficients characterizing the aerodynamic forces acting on the cylinder and details of the grids used. St is the shedding frequency, \bar{C}_D is the time-averaged drag coefficient, A_{C_D} and A_{C_L} are the maximum amplitude of the oscillations of the drag and lift coefficients respectively. All quantities are made non-dimensional by using L and the maximum velocity of the incoming flow.

Grid convergence tests were carried out in the two-dimensional simulations using three grids, mainly differing in the spatial resolution in the proximity of the cylinder. Details of the grids are reported in table 1. The grid GR4, used for the three-dimensional simulations, was built by replicating grid GR1 10 times in the spanwise direction (see table 1).

Since we intend to simulate an incompressible flow, the computations were performed by assuming that the maximum Mach number of the inflow profile is $M = 0.1$. This value allows compressibility effects to be neglected in the results.

In order to validate the numerical approach and to perform a grid convergence study, two-dimensional numerical simulations were carried out for $Re = 100, 180$ and 300 , on grids GR1, GR2 and GR3. The results were compared with those obtained for the same configuration in Breuer *et al.* (2000) and in Galletti *et al.* (2004), with different numerical methods and grid resolutions. The main bulk parameters characterizing the aerodynamic forces acting on the cylinder are shown in table 1; as can be seen the agreement with the results obtained in the literature is satisfactory. Moreover, it may be concluded that grid independence was almost reached, since in all cases the difference between the parameter values obtained with the different grids is very low ($\leq 2\%$, except for A_{C_D} , which is, however, almost negligible in most cases). Note that for the Strouhal number, St , the scatter between our results is lower than that between the data in the literature.

Three-dimensional simulations were carried out on grid GR4 at $Re = 300$. They are initiated from an impulsive start-up and the transient phase was recorded and analysed in order to investigate the mechanisms of formation of three-dimensional structures.

In figure 2(a) the time behaviour of the lift coefficient is shown. The values of the maximum and minimum spanwise velocity in the field are also reported as an indicator of the occurrence of three-dimensional phenomena in the flow. The three-dimensional effects on the aerodynamic forces are seen to be already significant soon after the vortex shedding phenomenon begins to take place, with a significant reduction of the

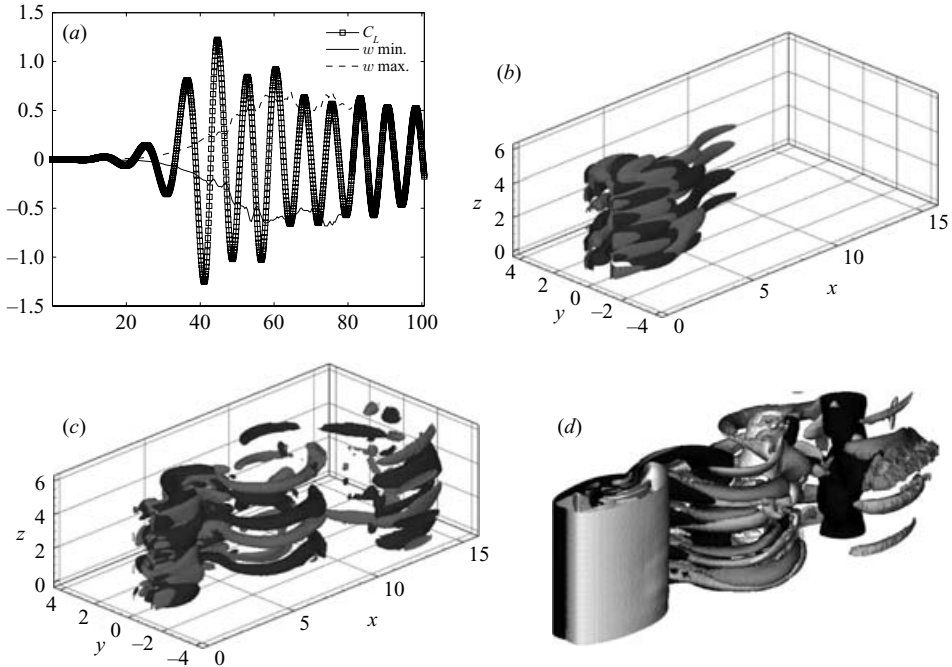


FIGURE 2. (a) Time variation of the lift coefficient and of the maximum and minimum of the spanwise velocity obtained in the three-dimensional simulation at $Re = 300$. (b) Streamwise vorticity in the wake obtained at $t \approx 35$. The grey and black surfaces correspond to $\omega_x = 0.05$ and $\omega_x = -0.05$ respectively. (c) Streamwise vorticity in the wake obtained at $t \approx 57$. The grey surface corresponds to $\omega_x = 0.4$ and the black to $\omega_x = -0.4$. (d) Streamwise and spanwise vorticity components in the wake obtained after the transient. The black and light grey surfaces correspond to $\omega_z = -0.4$ and $\omega_z = 0.4$ respectively. The streamwise tubes correspond to $\omega_x = 0.4$ and $\omega_x = -0.4$ respectively.

oscillation amplitude of C_L , due to the loss of coherence of the vortex shedding in the spanwise direction.

Let us now analyse in more detail the form of the three-dimensional instabilities and structures. Two different instability modes, initially identified in circular cylinder flows, have been found for unconfined square cylinders in experiments (Luo *et al.* 2003) and in the Floquet instability analysis (Robichaux, Balachandar & Vanka 1999). The first one, mode A, occurs at lower Re and is characterized by the formation of large-scale and wavy vortex loops that connect the spanwise von Kármán vortices. The other one, mode B, is characterized by shorter, finer-scaled vortex loops. For unconfined square cylinders, mode A was found to occur at $Re \approx 160$ with a spanwise wavelength of $5.2L$, and mode B at $Re = 190$ – 200 with a spanwise wavelength of $1.2L$. A third instability mode having a spanwise wavelength of $2.8L$ (mode S) was also identified through Floquet analysis, which was not, however, observed in the experiments.

From the early stages of transition, the flow structure is complex, as shown in figure 2b, in which two isosurfaces of the streamwise vorticity are shown at a time at which the spanwise velocity reached approximately 10% of the maximum inflow velocity. Mode-A-type structures tend to break into smaller vortical loops, but not yet showing a well-defined spanwise length. Later in the transient (figure 2c), only these smaller structures are visible, and they now have a much better defined periodical behaviour with a spanwise wavelength of approximately $1L$ and are, thus, probably

related to the instability mode B. These structures persist after the end of the transient (see figure 2d) and in the developed three-dimensional wake they connect the vortex tubes of the von Kármán street (in black and light grey in figure 2d). These spanwise vortex tubes are in turn corrugated and distorted by the motion induced by the streamwise vortices, and this is a typical scenario of three-dimensional wakes at moderate Reynolds numbers, both for unconfined circular and square cylinders (see Luo *et al.* 2003).

3. Low-order modelling

The possibility of reproducing a given dynamics is fundamental in devising even crudely approximated control laws by systematic means, e.g. optimal control theory. The main idea is to build a low-order model of an actuated flow from an existing database. Using this model, one computes the optimal actuation and applies it to the full approximation of the Navier–Stokes equations. If the error between this solution and that of the low-order model is not within a certain tolerance, then a new low-order model based on the latest Navier–Stokes solution is built. This iteration is performed until the error is within the tolerance. It has been shown that the loop converges under certain assumptions (Bergmann *et al.* 2005). Clearly, the crucial ingredient of this approach is to be able to accurately reproduce the observed dynamics.

To this end, the discrete instantaneous velocity is expanded in terms of discrete empirical eigenmodes: $\mathbf{u}(\mathbf{x}, t) = \bar{\mathbf{u}}(\mathbf{x}) + \sum_{n=1}^{N_r} a_n(t)\boldsymbol{\phi}_n(\mathbf{x})$, where $\bar{\mathbf{u}}(\mathbf{x})$ is a reference velocity field. The modes $\boldsymbol{\phi}_n(\mathbf{x})$ are found by proper orthogonal decomposition (POD) using the snapshots method of Sirovich (1987). Only a limited number of modes (N_r) is used in the representation of velocity; in the spirit of the POD, they are the modes giving the main contribution to the flow energy.

The numerical method used discretizes the Navier–Stokes equations for compressible flows. However, the Mach number considered is low ($M = 0.1$) and the flow can be considered as incompressible since the density fluctuations are negligible. Hence, the construction of the POD modes is based on the usual kinetic energy norm, and a Galerkin projection of the incompressible Navier–Stokes equations over the retained POD modes is carried out. This leads to the following low-order model:

$$\dot{a}_r(t) = A_r + C_{kr}a_k(t) - B_{ksr}a_k(t)a_s(t), \quad a_r(0) = (\mathbf{u}(\mathbf{x}, 0) - \bar{\mathbf{u}}(\mathbf{x}), \boldsymbol{\phi}_r) \quad (3.1)$$

where the Einstein summation convention is used, all the subscripts range from 1 to N_r and (\cdot, \cdot) denotes the canonical L^2 inner product. The coefficient B_{ksr} derives directly from the Galerkin projection of the nonlinear terms in the Navier–Stokes equations and it can be easily expressed in terms of the POD modes. The terms A_r and C_{kr} are calibrated using a pseudo-spectral method to take into account the pressure drop as well as the interaction of unresolved modes in the POD expansion. The calibration consists in solving an inverse problem where the coefficients A_r and C_{kr} are to be found such that the model prediction is as close as possible in the L^2 norm to the actual reference solution. This problem is solved using an accurate and efficient optimization method: accurate because the method is spectral, and efficient because the solution is obtained by solving a direct and an adjoint problem in one shot. See Galletti *et al.* (2005) for a detailed discussion.

In order to evaluate the possibility of modelling this flow by a reduced number of degrees of freedom, we consider two separate issues. As a first step, we *a priori* check if the flow admits a low-dimensional representation. In other words, we study the

POD case	Time interval	Number of snapshots
POD1	$382.24 < t < 397.61$	45
POD2	$360.23 < t < 412.64$	151
POD3	$94.38 < t < 412.64$	912
POD4	$5.3 < t < 59.45$	156

TABLE 2. POD database details.

approximation error of the flow snapshots as a function of the number of POD modes retained. Note that no dynamics is involved at this stage, it is merely a question of the POD modes actually spanning the solution manifold. The second issue concerns the error between the coefficients predicted by the calibrated model and the projection of the flow snapshots over the POD modes. This step is intended to verify if a quadratic model, where the nonlinear term is derived from the POD modes and the linear term is adjusted to fit the data, is capable of reproducing the dynamics of the flow.

With these objectives in mind, four different POD bases are computed using the flow snapshots obtained in the three-dimensional simulation at $Re = 300$. The first three (POD1, POD2 and POD3) are pertinent to the developed flow, i.e. when the three-dimensional structures in the wake are clearly developed. The fourth (POD4) is relative to the transient flow, i.e. when the three-dimensionality of the wake is developing.

The details of the snapshot databases used are summarized in table 2. The time-averaged flow field was subtracted from each snapshot before carrying out the PODs for the developed flow, while the two-dimensional unstable steady solution was subtracted from each snapshot for the transient case.

The main motivation for using a different number of flow snapshots for the developed flow is to show how the approximation properties of the POD modes depend on the flow database. To this end, we considered the reconstructed fluctuating energy for flow snapshots which are inside or outside the database used to determine the POD modes, figure 3 (*a-c*). The abrupt reduction of captured energy corresponds to snapshots which do not belong to the flow database. As the database becomes larger, this jump becomes smaller: as the number of flow snapshots in the database increases, the energy captured using a given number of modes increases for the snapshots outside the database as expected, while it decreases for the snapshots inside the database. This is a consequence of the chaotic nature of the flow and of the larger snapshot space to be represented.

Moreover we see that taking a larger number of modes to build the model makes sense only for larger databases. Large numbers of flow snapshots need to be taken into account to recover high levels of fluctuating energy outside the database, even in this case where the Reynolds number is small compared to real applications. However, the dimensional reduction is from $O(10^7)$ degrees of freedom to $O(10^2)$ for case (*c*), recovering about 70 % of the fluctuating energy outside the database. For the transient (figure 3*d*) we see that eight modes are enough to give a reasonable representation of energy.

Modes 1 and 3 relative to POD3 are shown in figure 4. The cylinder is not visualized, its axis being the intersection of the planes $x = 0$ and $y = 0$. The first mode is related to the classical vortex alley, although some corrugations due to three-dimensional effects are visible in the x - and y -components. The z -component is approximately one order of magnitude lower than the others, and it is at the threshold of numerical

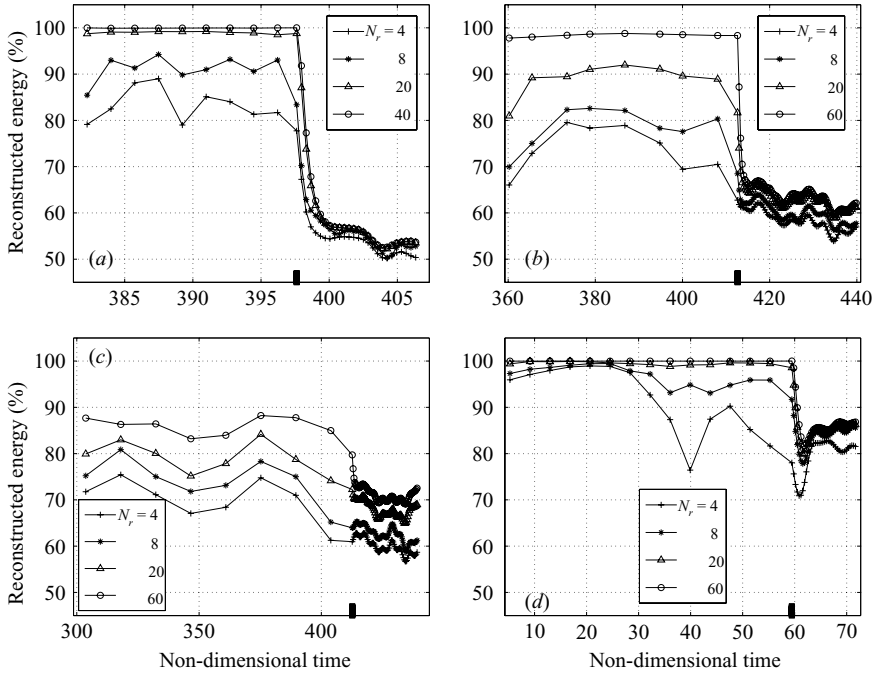


FIGURE 3. Percentage of reconstructed fluctuating energy for flow fields inside and outside the database. N_r is the number of modes. (a) POD1, (b) POD2, (c) POD3 and (d) POD4. $Re = 300$. The thick mark on the abscissa denotes the limit after which the reconstructed snapshots do not belong to the database.

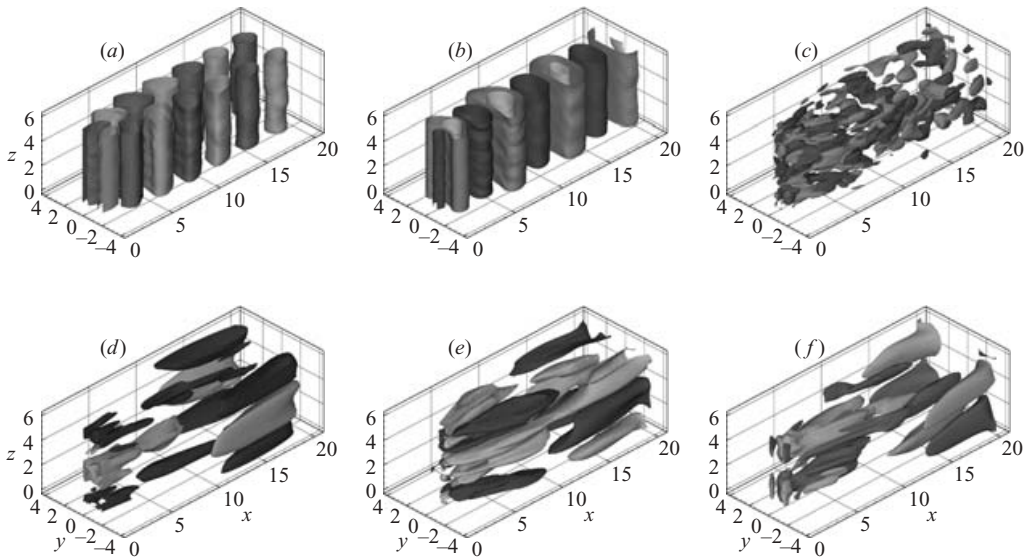


FIGURE 4. Components of the first (a–c) and third (d–f) mode relative to POD3. (a) x -component: light grey 0.015, dark grey -0.015 ; (b) y -component: light grey 0.05, grey 0.01, dark grey -0.04 ; (c) z -component: light grey 0.0035, dark grey -0.0035 ; (d) x -component: light grey 0.032, dark grey -0.032 ; (e) y -component: light grey 0.02, dark grey -0.02 ; (f) z -component: light grey 0.025, dark grey -0.025 .

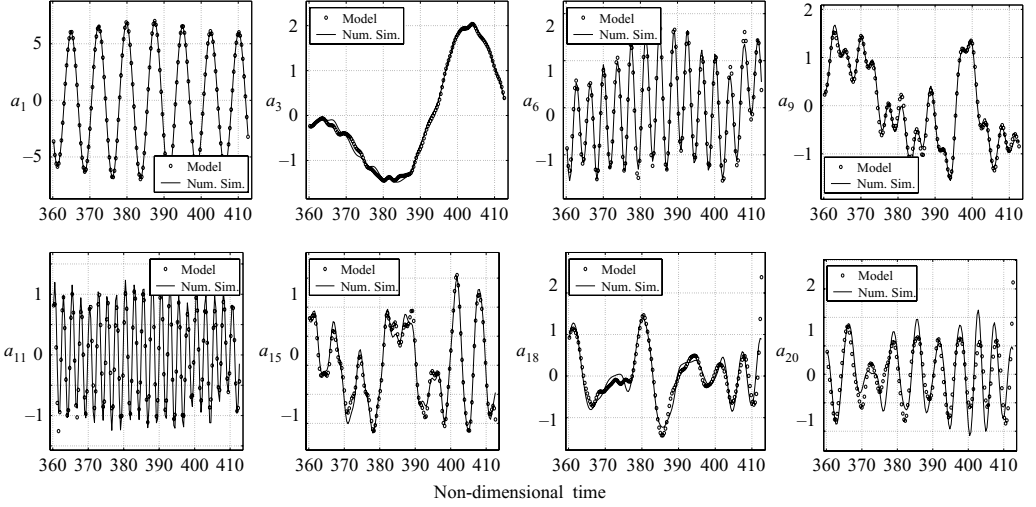


FIGURE 5. Developed three-dimensional flow: projection of the fully resolved Navier–Stokes simulations over the POD modes (continuous line) vs. the integration of the dynamical system obtained retaining the first 20 POD modes (circles). Only eight representative modal coefficients are shown here.

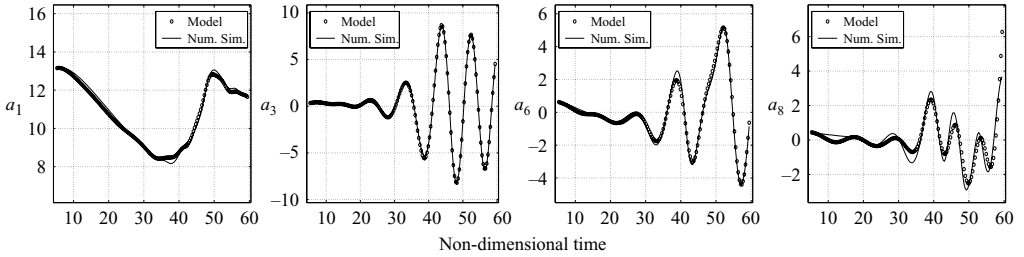


FIGURE 6. Transient after the impulsive start-up: projection of the fully resolved Navier–Stokes simulations over the POD modes (continuous line) vs. the integration of the dynamical system obtained retaining the first eight POD modes (circles). Only four representative modal coefficients are shown here.

noise. The main time frequency of the coefficient associated with this mode is that of the vortex shedding.

The third POD eigenfunction is of a different nature as it presents structures elongated in the x -direction. Moreover, all its components have the same order of magnitude. This mode appears to be related to the evolution of the three-dimensional instability and to the interaction with the bounding walls. In time, the frequency of the corresponding Galerkin coefficient becomes much lower. The subsequent modes are of the same kind as the ones depicted. They either represent smaller and smaller scales of vortex shedding, or finer three-dimensional structures.

For POD2 and POD4, the resulting dynamical systems were calibrated over the corresponding databases of table 2, using 121 and 81 collocation points respectively. A comparison between the model and the reference simulation was carried for the time-evolution of the POD modal coefficients and is shown in figures 5 and 6. The comparison was carried out for flow snapshots that are within the database used to compute the POD modes. Therefore, Figures 5 and 6 show how the low-order model fits the solution database from which the POD modes were derived.

The physical phenomenon is far from periodic. In the fully developed case we have low-frequency modulations as well as high-frequency bursts. In the transient case the spectrum is more compact but it is not steady. In both cases we are able to reproduce to a high level of accuracy the reference solution. As expected, the error is concentrated in the last modes, because the influence on these scales of the unresolved dynamics is higher. Since the simulation of the low-order dynamical system matches with good accuracy the reference results, it follows that the error in the physical space is of the order of the approximation error seen in figure 3.

An additional model was computed for POD1. In this case also the predictions are accurate compared to the reference solution. The model coefficients depend on the calibration database in a non-trivial way since they result in part from an inverse problem. However, it can be observed that in both POD1 and POD2 the matrix C_{kr} shows a pair of complex conjugate eigenvalues whose imaginary part is nearly equal to the frequency of the vortex shedding. The corresponding eigenvectors are mainly in the direction of the first and second POD mode. This feature was also observed in Galletti *et al.* (2005) for the two-dimensional instability leading to vortex shedding.

Finally, in the derivation of the reduced models, we are at present limited by the number of POD modes retained and the number of collocation points used to calibrate the flow (see Galletti *et al.* 2005 for details) because of the nonlinear optimization problem size: in the case of POD2 we solve an optimization problem with 5260 controls.

4. Concluding remarks

Accurate ‘plant models’ of flows whose dynamics are characterized by complex large-scale structures can be derived from simulation data sets. Within the range of calibration, the error between the flow predicted by such models and the reference solution is bounded. Moreover, it is of the order of the approximation error of the original data set projected over the POD modes, thanks to the pseudo-spectral approach employed. One result is hence that the adaptive control method proposed in Bergmann *et al.* (2005) could be applied in this case over time horizons of the order of 10 shedding cycles. However, the possibility of using calibrated POD models as a predictive tool seems to be very remote in cases like the present where the spatial and temporal complexity is important: the reconstruction error becomes relevant as soon as we take flow solutions that lie outside the snapshot range. Using $O(10^3)$ snapshots and 60 POD modes, the representation error is still of the order of 30% of the fluctuating energy. For this reason there will be an exponential divergence between any model prediction and the actual solution outside the snapshot range. Nonetheless one aspect is important: if the objective is to recover an estimate of the flow field from boundary measurements (for example a nonlinear observer), then such an error might still be acceptable.

In conclusion, the relevance of POD models based on the calibration procedure is that they can be used to determine control laws instead of the full Navier–Stokes equations, when the model includes the effect of the actuators. We mention that the grids used, their size and the number of flow snapshots can be representative of engineering problems, as a step to application of low-order models to practical flows.

This work was funded in part by the HPC-EUROPA project (RII3-CT-2003-506079). We thank M. Breuer for sharing his results with us, B. R. Noack, L. Cordier and C.-H. Bruneau for useful discussions, A. Dervieux and B. Koobus for making

available the core of the Navier–Stokes solver. IDRIS (Orsay, France), CINECA (Bologna, Italy) and M3PEC (Université Bordeaux 1, France) provided the computational resources. We are grateful to the “cellule informatique” at the Institut de Mathématiques de Bordeaux – in particular to P. Depouilly and S. Layrisse for their help with the data management.

REFERENCES

- BERGMANN, M., CORDIER, L. & BRANCHER, J.-P. 2005 Optimal rotary control of the cylinder wake using proper orthogonal decomposition reduced-order model. *Phys. Fluids* **17**, 097101.
- BREUER, M., BERNSDORF, J., ZEISER, T. & DURST, F. 2000 Accurate computations of the laminar flow past a square cylinder based on two different methods: lattice-Boltzmann and finite-volume. *Intl J. Heat Fluid Flow* **21**, 186–196.
- CAMARRI, S., SALVETTI, M. V., KOOBUS, B. & DERVIEUX, A. 2004 A low-diffusion MUSCL scheme for LES on unstructured grids. *Computers Fluids* **33**, 1101–1129.
- FARHAT, C., KOOBUS, B. & TRAN, H. 1999 Simulation of vortex shedding dominated flows past rigid and flexible structures. In *Computational Methods for Fluid-Structure Interaction*, pp. 1–30. Tapir.
- GALLETTI, B., BOTTARO, A., BRUNEAU, C. H. & IOLLO, A. 2005 Accurate model reduction of transient flows. *Tech. Rep. RR-5676* <http://www.inria.fr/rrrt/rr-5676.html>. INRIA.
- GALLETTI, B., BRUNEAU, C. H., ZANNETTI, L. & IOLLO, A. 2004 Low-order modelling of laminar flow regimes past a confined square cylinder. *J. Fluid Mech.* **503**, 161–170.
- GRAHAM, W. R., PERAIRE, J. & TANG, K. Y. 1998 Optimal control of vortex shedding using low-order models. Part I. *Intl J. Numer. Meth. Engng* **44**, 945–972.
- GUILLARD, H. & VIOZAT, C. 1999 On the behaviour of upwind schemes in the low Mach number limit. *Computers Fluids* **28**, 63–86.
- VAN LEER, B. 1977 Towards the ultimate conservative scheme. iv: A new approach to numerical convection. *J. Comput. Phys.* **23**, 276–299.
- LUMLEY, J. L. 1967 The structure of inhomogeneous turbulent flows. In *Atmospheric Turbulence and Radio Wave Propagation* (ed. A. M. Yaglom & V. L. Tatarski), pp. 166–178.
- LUO, S., CHEW, Y. & NG, Y. 2003 Characteristics of square cylinder wake transition flows. *Phys. Fluids* **15**, 2549–2559.
- MA, X. & KARNIADAKIS, G. E. 2002 A low-dimensional model for simulating three-dimensional cylinder flow. *J. Fluid Mech.* **458**, 181–190.
- ROBICHAUX, J., BALACHANDAR, S. & VANKA, S. P. 1999 Three-dimensional Floquet instability of the wake of square cylinder. *Phys. Fluids* **11**, 560–578.
- ROE, P. 1981 Approximate Riemann solvers, parameters vectors, and difference schemes. *J. Comput. Phys.* **43**, 357–372.
- SAHA, A. K., BISWAS, G. & MURALIDHAR, K. 2003 Three-dimensional study of flow past a square cylinder at low Reynolds number. *Intl J. Heat Fluid Flow* **24**, 54–66.
- SIROVICH, L. 1987 Turbulence and the dynamics of coherent structures. Parts I,II and III. *Q. Appl. Math.* **XLV**, 561–590.
- SOHANKAR, A., NORBERG, C. & DAVIDSON, L. 1999 Simulation of three-dimensional flow around a square cylinder at moderate Reynolds numbers. *Phys. Fluids* **11**, 288–306.
- TELIB, H., MANHART, M. & IOLLO, A. 2004 Analysis and low-order modeling of the inhomogeneous transitional flow inside a T-mixer. *Phys. Fluids* **8**, 2717–2731.